Understanding the Temporal Dynamics of Coherence and Backscattering Using Sentinel-1 Imagery for Crop-Type Mapping

Qinxin Zhao, Qinghua Xie, Xing Peng, Kunyu Lai, Jinfei Wang, *Member, IEEE*, Haiqiang Fu, *Senior Member, IEEE*, Jianjun Zhu, and Yang Song

***Abstract*—This study investigates the application of coherence and backscattering, derived from time-series Sentinel-1 synthetic aperture radar imagery of a crop season (18 scenes with a 12-day revisit cycle), for crop growth monitoring and classification in the agricultural region of Southwestern Ontario, Canada. To fulfill this goal, we initially analyze the temporal behavior of backscattering and coherence for a variety of crops to gain some insights for classification. Second, diverse combinations involving polarization channels, feature types, and image quantities for crop classification are analyzed. The deep analysis of temporal dynamics highlights a stronger correlation between the time-series curves of backscattering and crop growth in comparison to coherence. The VH backscattering and the VV coherence demonstrate a higher sensitivity to the variations in crop growth. The crop mapping results indicate that backscattering produces significantly higher accuracy of crop classification than coherence. Furthermore, the incorporation of coherence features with backscattering can enhance the accuracy, with VV making more pronounced contributions compared to VH. Notably, the most effective classification result is achieved through a scheme that integrates both backscattering coefficients of dual polarization (VV + VH) and the VV coherence, achieving a better overall accuracy of 95.33% and a kappa coefficient of 0.93. This study concludes that the crucial information provided by the temporal variations in backscattering and coherence to improve crop classification accuracy depends on both the polarization channel and crop type, with coherence playing a supplementary role. Our study consolidates the previous work and provides useful insights into the field of crop classification.**

***Index Terms*—Agriculture, crop classification, crop monitoring, interferometric coherence, polarimetric backscattering, synthetic aperture radar (SAR), time-series.**

Manuscript received 22 November 2023; revised 5 February 2024 and 26 February 2024; accepted 28 February 2024. Date of publication 5 March 2024; date of current version 22 March 2024. This work was supported in part by the National Natural Science Foundation of China under Grant 42171387, Grant 41820104005, Grant 41804004, and Grant 42101400, in part by the Canadian Space Agency SOAR-E Program under Grant SOAR-E-5489, and in part by the Natural Science and Engineering Research Council of Canada Discovery Grant under Grant RGPIN-2022-05051. *(Corresponding author: Qinghua Xie.)*

Qinxin Zhao, Qinghua Xie, Xing Peng, and Kunyu Lai are with the School of Geography and Information Engineering, China University of Geosciences, Wuhan 430074, China (e-mail: qinxinzhao@cug.edu.cn; xieqh@cug.edu.cn; pengxing@cug.edu.cn; lky@cug.edu.cn).

Jinfei Wang is with the Department of Geography and Environment, the University of Western Ontario, London, ON N6A 5C2, Canada (e-mail: jfwang@uwo.ca).

Haiqiang Fu and Jianjun Zhu are with the School of Geosciences and Info-Physics, Central South University, Changsha 410083, China (e-mail: haiqiangfu@csu.edu.cn; zjj@csu.edu.cn).

Yang Song is with the Zoomlion Smart Agriculture, Company Ltd., Changsha 410205, China (e-mail: songyang@zoomlion.com).

This article has supplementary downloadable material available at https://doi.org/10.1109/JSTARS.2024.3373489, provided by the authors.

Digital Object Identifier 10.1109/JSTARS.2024.3373489

I. Introduction

THE quantity and quality of arable land have been increasingly threatened by natural and man-made factors. A certain correlation exists between the mapping of arable farmland and crop species [1], [2]. In this regard, the spatial distribution data of crops becomes crucial for effective agricultural monitoring and management, enabling the achievement of high productivity, high yields, and energy conservation in sustainable agricultural development [3], [4], [5]. Addressing contemporary challenges, modern agricultural technology facilitates effective management of agricultural production activities and monitoring of crop cultivation [6], [7], [8].

Remote sensing technology is an important tool to guide crop growth, optimize planting structure, and guarantee food security in modern agricultural technology. It can complement or replace traditional field surveys. With the advantages of high resolution, low cost, and wide coverage, it has the ability to obtain crop planting structure, area, and spatial distribution in a timely and accurate manner [2], [9], [10]. In particular, synthetic aperture radar (SAR) imagery excels as an active microwave remote sensing technique, and it has the following advantages over optical imagery [11]:

1) all-weather, all-day, and all-time data acquisition capability, suitable for temporal analysis;
2) strong penetration capabilities through vegetation, soil, and dry snow with minimal atmospheric interference;
3) multiple polarization channels enhancing sensitivity to observe earth surface scattering mechanisms;
4) interferometric capabilities enabling temporal information extraction from coherence analysis.

In recent years, the utility of SAR in the realm of agriculture has been substantiated, encompassing a spectrum of applications, including crop monitoring [12], [13], [14], crop classification [15], [16], [17], crop rotation identification [18], crop change detection [19], and so on. These extensive research efforts and applications indicate that SAR imagery not only provides surface information but also rich internal structural details. Consequently, SAR imagery serves as a high-quality

source in crop classification studies [15], [20]. At present, there are two distinct types of information used by SAR images for crop mapping: polarization features and interferometric features.

On account of polarimetric SAR (PolSAR) having exceptional sensitivity to the physical structure and dielectric properties of targets, the backscattering coefficients, as the fundamental polarimetric feature, have been widely used in crop-type mapping studies [21], [22]. The advancement of radar technology has led to the refinement of polarimetric channels and revisit cycles, with crop classification research transitioning from single-polarization and single image [23] to multipolarization and multitemporal [24]. Comparative analysis of single-polarization, dual-polarization, and quad-polarimetric data in [25] reveals the superiority of multipolarization in crop classification, while the differentiation between dual-polarization and full-polarimetric is minimal when utilizing time-series images spanning the entire crop growth cycle. However, previous studies have demonstrated the great advantage of quad-polarimetric in distinguishing crop types and monitoring crop phenology [26], considering the difficulty of data acquisition, as well as its high cost, and that the temporal features can make up for the differences between quad- and dual-polarization. Therefore, dual-polarization Sentinel-1 data are considered sufficient for accurate crop classification. By using multitemporal Sentinel-1 dual-pol backscattering for crop mapping, the majority of crops were successfully identified with satisfactory results [21], [27], [28].

As known, the coherence of interferometric SAR (InSAR) quantifies temporal changes in scattering characteristics between acquisitions, which can unveil the dynamics of scattering properties for different land-cover types [29]. Thus, coherence can provide better benefits for land-cover classification efforts [30]. Since crops undergo notable variations throughout their different growth phases, including vegetation coverage, crop height, leaf area, and other parameters, crops exhibit distinct characteristics compared to the rest of the land-cover types. Research works by Engdahl and Hyyppa [31] and Blaes and Defourny [32] pioneered the use of ERS-1/2 interferometric data for land-cover classification and crop growth monitoring. It is obvious that coherence provides distinct crop information compared to backscatter coefficients, offering a unique perspective to enhance crop separability. The study by Ramsey III et al. [33] presented that SAR coherence provides better discrimination over backscattering between land-cover types at some specific periods (e.g., off-season of defoliation, etc.). Similarly, there was a significant correlation between crop growth cycles and coherence, with a descending trend during the growth period of plants and high coherence values before planting and close to harvest time [34]. Recent research works expand coherence application to various regions and crops. The study in [35] assessed the suitability of coherence as a crop monitoring tool by means of multiyear Sentinel-1 coherence time series, taking into account 18 vegetation types. It also reveals that coherence correlates well with the normalized difference vegetation index derived from Sentinel-2 images. Hence, the study by Villarroya-Carpio et al. [36] explored Sentinel-1 coherence as a new radar vegetation index for crop monitoring and verified the performance within 16 distinct crop species. Among them, the coherence from the VV channel was proven as the optimal choice for describing crop evolution due to its higher correlation.

Considering both advantages, combining interferometric coherence with backscattering features was naturally concerned and successfully applied for the moisture estimation of soil and crop [37], [38] and land-cover classification, such as in wetland [39] and grassland areas [40], [41]. For crop classification, there are also some cases in previous studies. In the study of [42], the added value of coherence was demonstrated in the improved crop sensitivity at the harvesting stage and in addressing the challenge of distinguishing crops from herbaceous vegetation. In [43], the additive contributions of single-pass coherence and repeat-pass coherence on the backscattering coefficient of the TanDEM-X data for crop classification were examined. In [44] and [45], the synergistic use of backscatter and coherence of the dual-pol Sentinel-1 was used to generate thematic maps for crop classification, which showed that the incorporation of coherence contributed to the improvement in the classification accuracy using backscattering features alone. In addition, the coherence of co-pol is more sensitive to changes in crop growth than cross-pol.

In spite of the existence of Sentinel-1 studies based on coherence and backscattering features for crop classification, most of them employed data with a 6-day revisit cycle [30], [38], [44], [45], while a few studies used data with a 12-day revisit cycle [34]. The temporal analysis and crop classification in these studies were often treated as independent aspects, with limited efforts to interlink them for comprehensive interpretation. Moreover, the impact of the image numbers on backscattering utilization and the phenological period on coherence utilization for crop classification were poorly documented in previous studies. In addition, agricultural activities and climate conditions vary across regions, such as crop rotation and snow cover period. Therefore, utilizing the backscattering and interferometric coherence for crop monitoring and classification needs to be further explored to acquire additional useful insights.

In this context, the motivation of the study is to investigate the time-series dynamics in SAR backscattering and coherence, aiming to gain insights into understanding crop mapping while evaluating the effectiveness enriched by interferometry. The time-series C-band Sentinel-1 SAR imagery with a revisit cycle of 12 days, covering the period from April to October 2018 over the agricultural region of Southwestern Ontario, Canada, was collected. The major innovations and contributions of this study are summarized as follows.

1) We provide a comprehensive understanding of the temporal behaviors of backscattering and coherence, along with the relationship between each other among three primary crops under local farming practices.
2) We consolidate the idea that SAR data for crop classification go beyond backscattering coefficient and can be complemented by interferometry. We also evaluate classification performance using various features and explore a refined crop classification scheme.
3) We analyze the effects of the number of images and the phenological period on crop classification using backscattering and coherence individually.

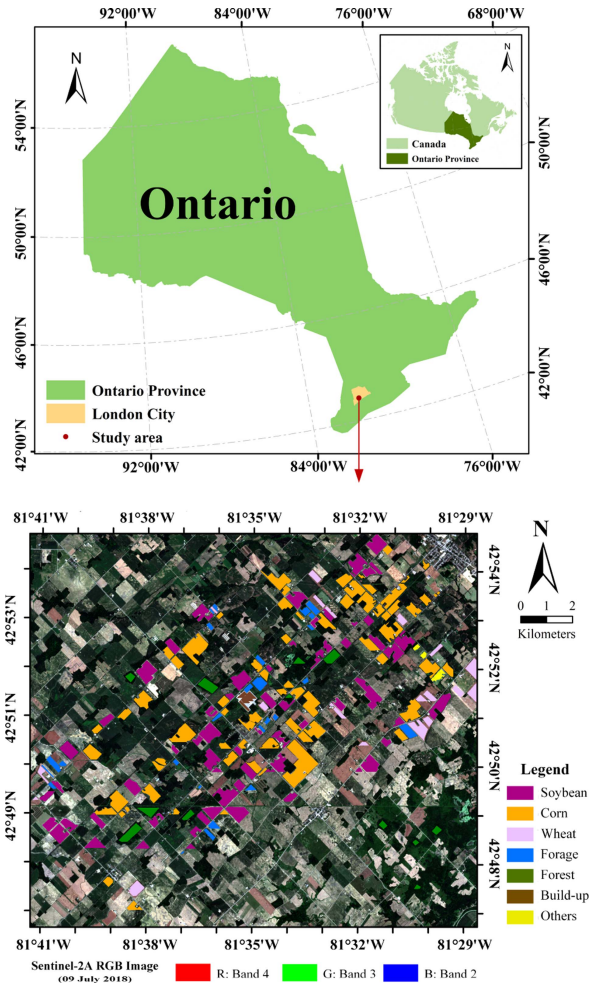

Fig. 1. Geographical location of the study area, RGB image of the Sentinel-2 data acquired on 09/07/2018 (Red: B4, Green: B3, Blue: B2), and ground truth data.

II. Materials and Methods

A. Test Sites

The study area is situated in the farmland area of Komoka (42°56'55" N, 81°26'10" W), to the west of London, Ontario, Canada. Fig. 1 illustrates the exact location of the study area and the RGB image of the Sentinel-2 data acquired on July 9, 2018. Due to its mild climate, adequate water supply, and fertile soil, the study area ensures a beneficial growing environment for crops as well as a long growing season, which makes it possible to carry out crop classification studies with great efficiency. Within the agricultural region, there exists a mixed woodland ecological zone, consisting of both farmland and woodland. The primary crops cultivated in this area include winter wheat, corn, soybean, and forage crops such as alfalfa, and grass. Furthermore, given their limited sample sizes, both tobacco and squash were consolidated into other classes. It should be noted that the study area is covered with snow from November to March each year. During this period, winter wheat is in a dormant state (overwintering), ceasing active growth. Nutrients are stored in the roots during this time, and the sufficient nutrients provided during the spring green-up, which occurs when the snow melts in April, ensure the yield of winter wheat.

TABLE I
Number of Polygons and Total Pixels in the Sample Datasets

Class	Polygons	Training pixels	Testing pixels
Soybean	80	60 000	40 000
Corn	104	66 000	44 000
Wheat	20	11 400	7600
Forage	29	9000	6000
Forest	13	7500	5000
Build	5	1440	960
Other	10	1110	740
	Total:261	Total: 156 450	Total: 104 300

B. Field Survey

As shown in Fig. 1, the 2018 reference dataset was assigned crop label values after field collection from April to October by the Geographic Information Technology and Applications Laboratory at the University of Western Ontario. Furthermore, the crop planting structure in the study area exhibits negligible fluctuations during the data collection period, rendering them inconsequential and permitting the assumption that the assigned category labels for each land parcel remained valid throughout the year 2018. Table I presents detailed information about the reference dataset, including the number of vector polygons, training pixels, and the testing pixels for each crop type. Each pixel corresponds to an area of 10 m $\times$ 10 m. In addition, the total area of the study area is about 269.0473 km^2. The smallest field area is 0.021 km^2 and the largest field area is 1.0587 km^2 in our field surveying.

In the study area, the sowing and harvesting periods of the predominant crops (corn, soybean, and winter wheat) exhibit an annual synchrony. Corn and soybean adhere to a synchronized timetable: sowing commences in May, reaching full maturity by September, and culminating in a harvest during the month of October. In contrast, winter wheat follows a distinct planting schedule, with seeds typically sown in October of the preceding autumn. The harvest time is typically conducted from the latter part of July to the early days of August in the subsequent year. Remarkably, the practice of crop rotation prevails in this region, resulting in discernible disparities between residues from the previous year's harvest and the crops sown in the current year. These residual materials play a crucial role in soil fertility and ameliorating water resource conservation. For instance, it is common to find residues from corn or soybean present in winter wheat fields prior to land preparation for sowing. We have provided approximate phenological ranges for three crops in Table II based on local agricultural practices and the general pattern of crop growth (similar each year). Fig. 2 roughly displays the actual phenological stages of soybean, corn, and winter wheat within the study area.

C. Sentinel-1

The SAR images were acquired from the C-band Sentinel-1 satellite in interferometric wide mode employing TOPSAR technology. Due to snow cover from November to March and only

TABLE II
APPROXIMATE DATES OF EACH PHENOLOGICAL STAGE FOR THE THREE CROPS

	Plowing	Seeding	Leaf development	Stem elongation	Booting	Maturity	Harvest
Soybean	80–122	123–143	144–179	180–199	200–234	235–258	259–320
Corn	80–117	118–138	139–170	171–190	191–232	233–265	266–320
wheat	--	--	80–132	133–167	168–194	195–210	211–232

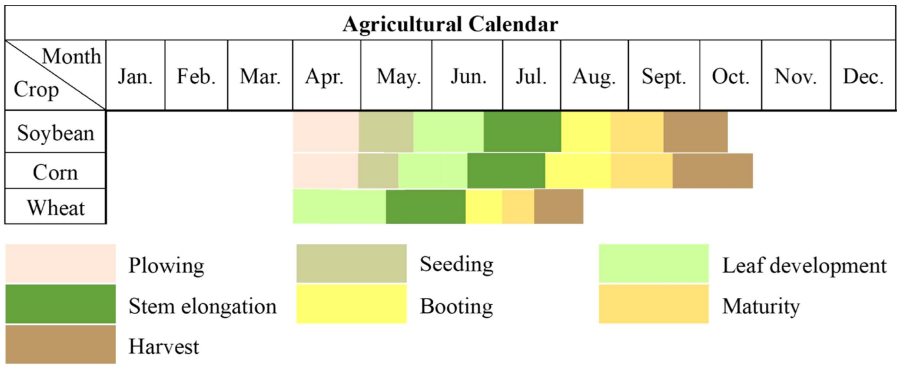

Fig. 2. Phenological stages of soybean, corn, and winter wheat within the study fields in 2018.

TABLE III
MAIN IMAGING PARAMETERS OF TIME-SERIES SENTINEL-1 IMAGES

Parameters	Information
Satellite	Sentinel-1A
Flight Direction	Ascending
Polarization Mode	VH + VV
Incidence Range	30.3°-42.8°
Azimuth Pixel Spacing	13.94 m
Range Pixel Spacing	2.33 m
Available Dates	20180404, 20180416, 20140428, 20180510, 20180522, 20180603, 20180615, 20180627, 20180709, 20180721, 20180802, 20180814, 20180826, 20180907, 20180919, 20181001, 20181013, 20181025

images with a revisit time of 12 days available in the study site, we finally acquired 18 Sentinel-1 single look complex (SLC) ascending images in dual-polarization channels (VV and VH), spanning from 4 April to 25 October in 2018, encompassing the main growing season of crops. Consequently, a total of 17 interferometric image pairs, spaced at a temporal interval of 12 days, were obtained. The main imaging parameters of time-series Sentinel-1 images are presented in Table III.

D. Backscattering Intensity and Interferometric Coherence

1) Backscattering: The backscattering coefficient, as a pivotal attribute of PolSAR imagery, effectively reflects the intrinsic characteristics of objects. The backscattering coefficient σ_0 is a measure of the intensity of electromagnetic radiation that is scattered back toward the radar after interacting with a target. For the Sentinel-1 dual polarization channel, two backscattering coefficients can be obtained (e.g., VV and VH in this study), which elicit distinct responses from terrestrial objects. As the growth structure of crops varies across different stages, the temporal series of backscattering intensity values exhibit seasonal trends related to growth cycles. To effectively analyze the backscattering coefficient and highlight changes in crop scattering characteristics, transforming it logarithmically is usually performed by

$$\sigma_0\ (\mathrm{dB}) = 10 \times \log_{10}(\sigma_0) \tag{1}$$

where $\sigma_0(\mathrm{dB})$ is the value of the backscattering coefficient in decibel.

2) Coherence: Coherence serves as a fundamental attribute within InSAR images, enabling an evaluation of the dynamics of scattering properties between two acquisitions over the same region and the phase quality of interferograms. The coherence magnitude (ρ) between two SAR images is usually estimated employing maximum likelihood methodology over a moving

window, which can be defined as [46], [47]

$$\rho = \frac{\left|\sum_{n=1}^{N} S_1 S_2^*\right|}{\sqrt{\left(\sum_{n=1}^{N} S_1 S_1^*\right) \cdot \left(\sum_{n=1}^{N} S_2 S_2^*\right)}} \tag{2}$$

where S_1 and S_2 denote the master and slave images, respectively, and N is the number of samples of the moving window. $|\,|$ signifies the absolute value operator, while $*$ represents the complex conjugate. The range of ρ spans from 0 to 1. As scattering properties from the master and slave images are completely correlated, ρ reaches its maximum value of 1. On the contrary, when ρ approaches 0, it signifies that the two SAR images are uncorrelated.

This work focuses on the significance of temporal coherence, a product of interferometric pairs generated by consecutive images, as an additional feature in crop classification. With n scenes of SAR images, it is possible to acquire the coherence of n-1 interferometric pairs. The corresponding time-series coherence (TC) is defined by means of a row vector as follows:

$$\mathrm{TC} = \left[\begin{array}{cccc} \rho_{12} & \rho_{23} & \cdots & \rho_{(n-1)n} \end{array}\right]. \tag{3}$$

However, coherence is influenced by a multitude of factors. For land-cover classification, the emphasis is placed on the temporal decorrelation, which manifests as the phase disparity between the two backscattering signals owing to alterations in the physical properties of the Earth's surface or the position of scatterers within the temporal interval linking two observations. In the case of crops, the degree of coherence tends to decrease when the crop undergoes variations in its growth cycle between the acquisition of two SAR images. Conversely, if the covered elements remain unchanged during the acquisition period, the degree of coherence is significantly higher.

E. Preprocessing

In this study, all the Sentinel-1 image preprocessing tasks were expertly performed using the Sentinel Application Platform software, developed by the European Space Agency (ESA) [48]. The processing flow used to obtain the backscattering coefficients and interferometric coherence is shown in Fig. 3.

The preprocessing of the backscattering coefficient derived from the 18 scenes of SLC images mainly includes a number of steps: TOPSAR Split, Orbit correction, Radiometric calibration, TOPSAR deburst, Multilooking processing with 3-looks in range dimension and 1-look in azimuth dimension, Geocoding, Speckle filter (9 × 9 boxcar), and Conversion from linear to dB. By means of the above preprocessing steps, the $\sigma_0(\mathrm{dB})$ images for both VV and VH polarizations in the UTM system are obtained, with a resolution of 10 m × 10 m. Notably, due to the flat terrain and the large field size in our study area, the preprocessing approach of speckle filtering after terrain correction employed in this study is acceptable. However, conducting terrain correction as the final preprocessing step is a general principle, which could avoid the effects of changes in the statistics of the data wherever there is no one-to-one correspondence that may arise due to terrain correction, especially in the presence of slopes.

The interferometric preprocessing steps mainly consist of: TOPSAR split, Orbit correction, Radiometric calibration, Image coregistration, Speckle filtering and coherence estimation using a window of 3 × 10 (azimuth × range), TOPSAR deburst, Multilooking processing with 3-looks in range dimension and 1-look in azimuth dimension, and Geocoding images to UTM system with a resolution of 10 m × 10 m.

Following the above steps, the backscattering coefficient and coherence derived from the preprocessing of multitemporal Sentinel-1 data were stacked separately using the layer stacking function. This resulted in composite images comprising all backscattering for a single polarization (VV or VH), each with 18 layers. Similarly, composite images were generated for all coherence images for a single polarization, each containing 17 layers.

F. Classification Method and Evaluation

In this study, the random forest (RF) algorithm was employed for classification tests using the intensity and coherence features of Sentinel-1 images, both individually and in combination. RF is an integrated machine learning algorithm [49], frequently used in remote sensing due to its high accuracy and stability compared to individual classifiers [50]. RF consists of multiple decision trees, each independently trained on a randomly selected subset of the original data. Moreover, these trees autonomously acquire the capacity to generate predictions and cast votes for their respective categories. By using the vote results, the category with the highest number of votes is designated as the classification result.

In this study, the RF classifier was furnished by the scikit-learn toolkit in the Python language [51]. Multiple adjustable parameters exist for the RF classifier, such as the number of decision trees (n_estimators) to create per class, the minimum number of samples for the branch node (min_samples_split), and the minimum sample size of the leaves (min_samples_leaf). Among them, previous studies have shown that the classification accuracy using an RF classifier tends to stabilize as more than 50 decision trees are used [16], [52], [53]. In addition, 100 decision trees proved to be sufficient in crop classification in the same study area as ours, which performed well [15], [16]. The remaining parameters play a relatively minor role in the context of crop classification. In this study, 100 decision trees were employed in the RF algorithm for all classification tests, while the other parameters were kept at default settings in the scikit-learn software package (min_samples_split = 2, min_samples_leaf = 1).

Due to the fact that neighboring pixels within the same field are highly correlated [54], the dataset needs to be partitioned at the field level rather than the pixel level. The dataset was divided into five subsets numbered 1–5, and the same number of pixels in each subset were chosen. After that, two subsets (40%) of the datasets were used as testing data, and the remaining three subsets (60%) of the datasets were used as training data. To minimize classification uncertainty, such combinations were repeated five times. Fig. 4 shows the five training sets used in our classification experiments and the corresponding testing sets.

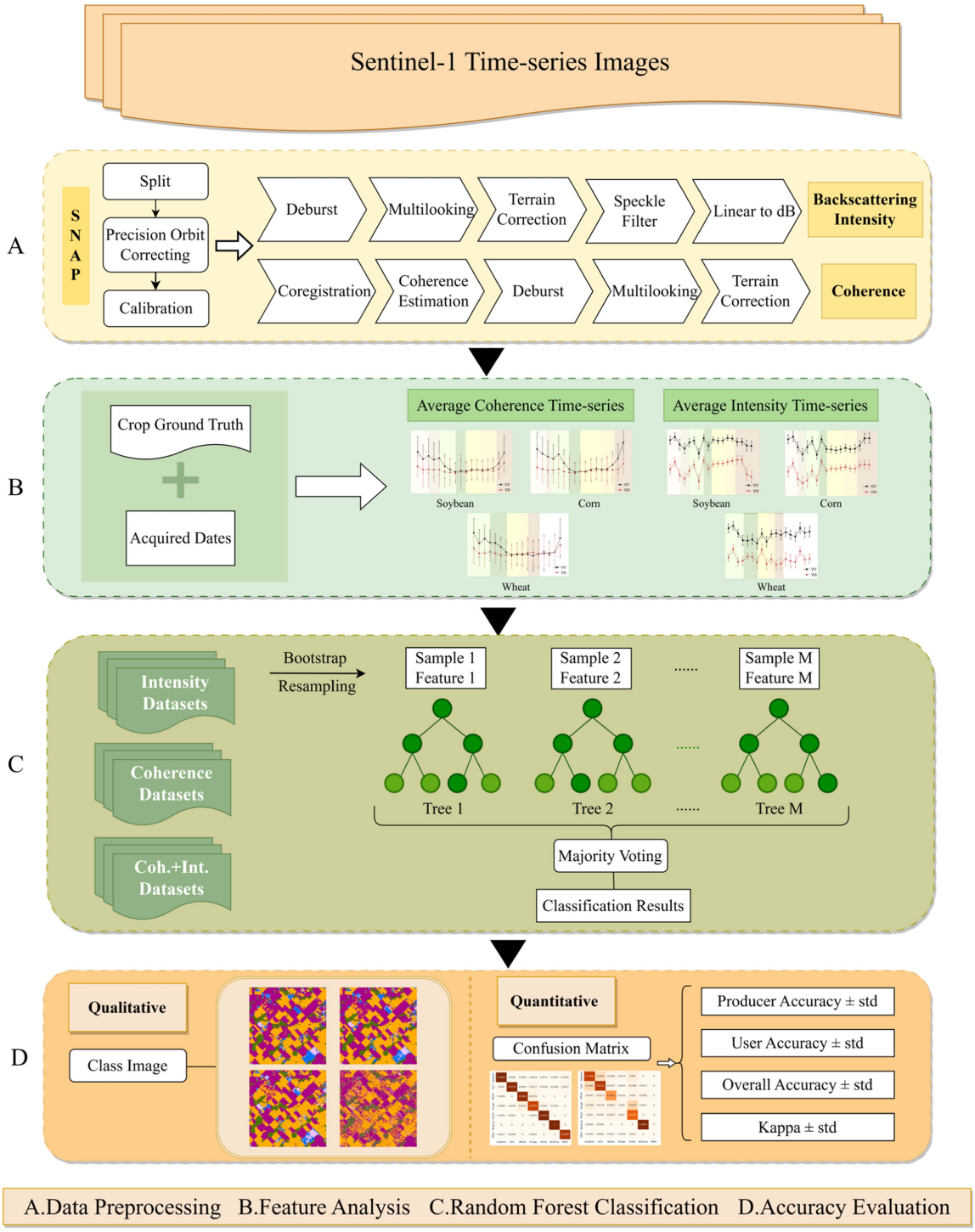

Fig. 3. General technical flowchart of this study.

The corresponding numbers under the images are the number of subsets used.

To quantitatively assess the performance of classification, confusion metrics were employed, including overall accuracy (OA), kappa coefficient [55], producer's accuracy (PA), and user's accuracy (UA) [56]. Among them, OA is the ratio of the correctly predicted instances to the total number of instances in all test sets for a model, and the kappa coefficient is a commonly used method for assessing interrater reliability. Notably, PA elucidates the likelihood of correctly classifying the ground truth data for a crop category, and the UA refers to the probability of the crop classification results matching the actual type. In other words, PA corresponds to the omission error, and UA corresponds to the commission error. In consideration of five rounds of classification, each involving separate training and testing sets, we calculated the mean and standard deviation

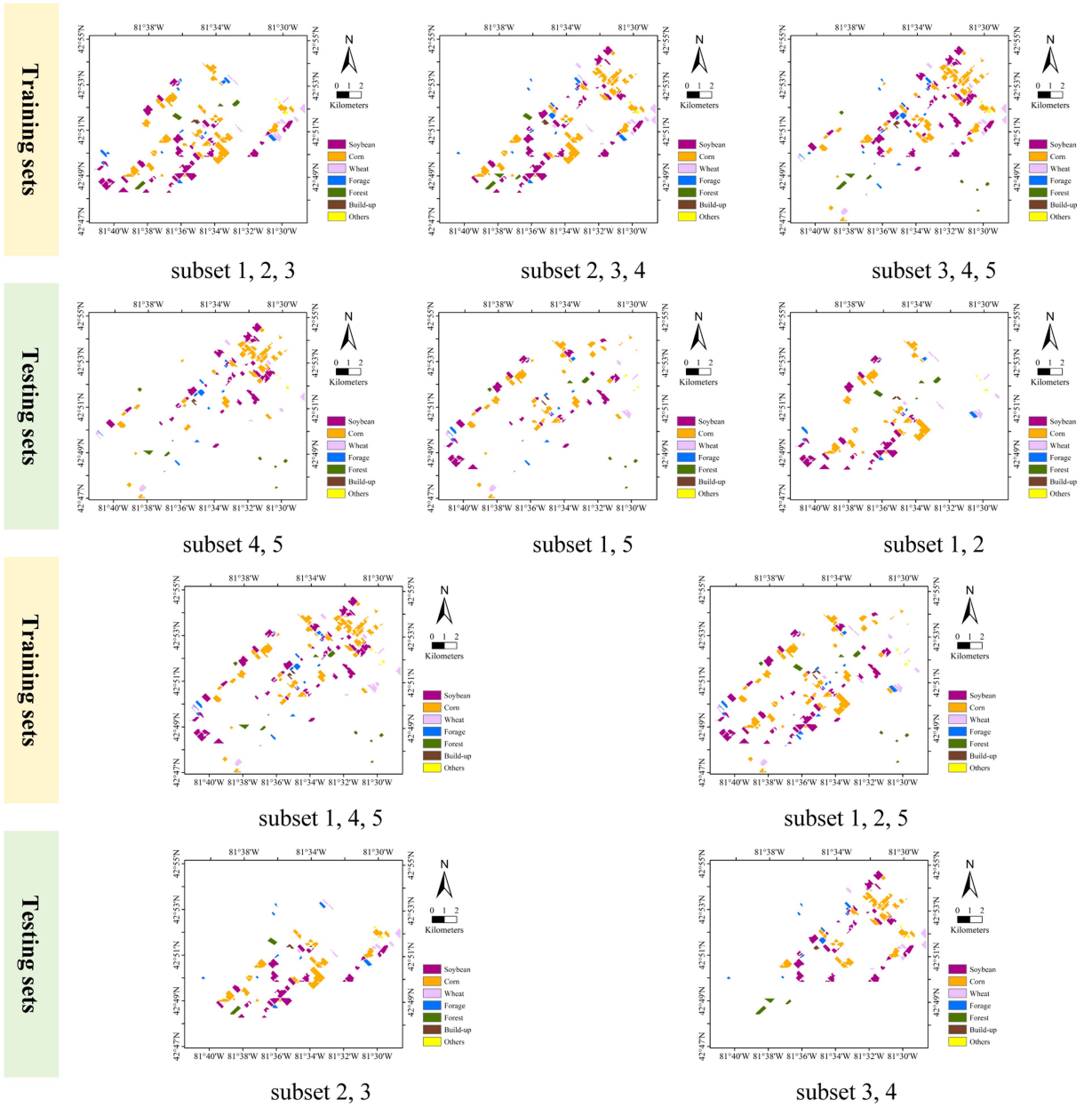

Fig. 4. Five training sets used in classification experiments and the corresponding testing sets.

(STD) of each indicator. This calculation was performed to assess the robustness and reliability of the results.

III. Time-Series Dynamics of Features

As we used backscatter coefficients and coherence as input features for crop classification, it was essential to examine the temporal dynamics of two features throughout the growth cycle of major cash crop types in the 204 fields, comprising 80 soybean, 104 corn, and 20 winter wheat fields. Hence, Fig. 5 reveals the temporal evolution of the mean backscattering intensity and coherence values for all fields corresponding to the three types of crops throughout the entire growth cycle, along with their STDs. The detailed values obtained from backscattering and coherence to demonstrate the microwave responses to different phenological stages of crops are presented as supplementary data.

A. Backscattering

As illustrated in Fig. 5, the backscattering values obtained from VV and VH exhibit fluctuant and analogous temporal patterns across the growth cycle of the three crops, which presents the average values and corresponding errors (error bars) for all fields of the same crop type. As expected, the magnitudes from co-pol channel (VV) are always higher than the cross-pol channel (VH) due to the depolarization effect [44]. In VV polarization, the intensity values of various crops range from

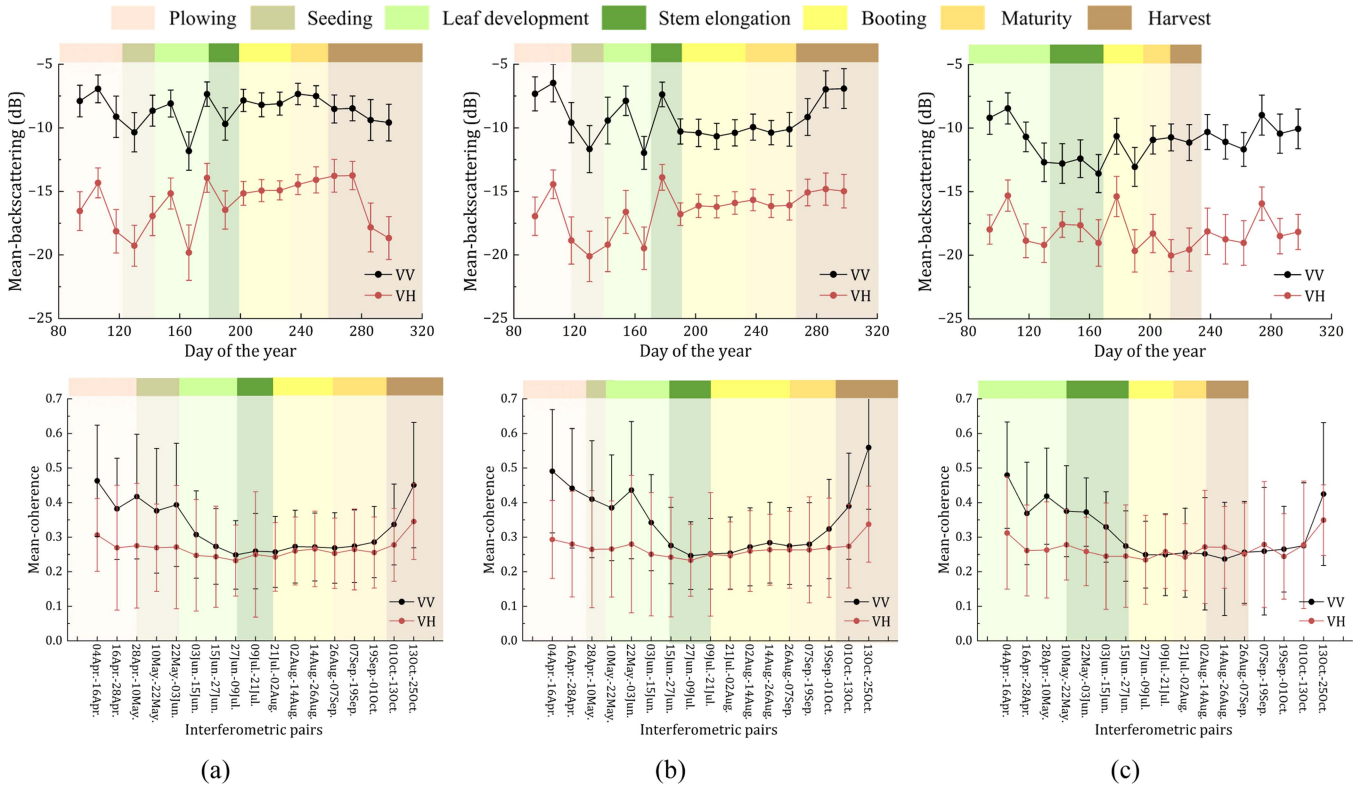

Fig. 5. Temporal evolution of the backscattering intensity and the interferometric coherence at VV and VH channels. (a) Soybean. (b) Corn. (c) Wheat.

−14 to −6 dB, while in VH polarization, the intensity values are relatively smaller, ranging from −21 to −13 dB. Importantly, there is a greater difference between the maximum and minimum values for each crop in VH (around 7 dB) compared to VV (around 5 dB).

Between early April and the beginning of May, three types of crops display very similar patterns. In April, as a result of melting snow and the emergence of crop residue, both soil moisture content and soil roughness increased. However, the backscattering is sensitive to soil characteristics such as moisture and roughness, leading to a slight increase in VV and VH backscatter values. Then, a decline in VV and VH backscatter values is evident until the beginning of May. This decrease can be attributed to the attenuation of soil backscatter caused by the plowing, seeding, and growing vegetation, possibly coupled with the gradual smoothing of the soil surface [14]. As the season advances, disparities between summer and winter crops start to become apparent.

For summer crops (soybean and corn), their growth patterns are roughly similar, which is consistent with [15]. During May to early June, the crop transitions from seeding to nurturing leaves, and the increase in biomass leads to an upward trend in backscattering values. For soybeans, the VV values exhibited an increase from −10 to −8 dB, while the VH values rose from −19 to −15 dB. Similarly, for corn, the VV values showed an increase from −12 to −8 dB, and VH values increased from −20 to −17 dB. In mid-June, as the leaves of these crops began to grow laterally, the influence of the underlying soil diminished and most of the scattering occurred on the leaf surfaces. Consequently, the backscattering values experienced a substantial reduction during this stage. For soybeans, the VV values decreased from −8 to −12 dB, and VH values dropped from −15 to −20 dB. For corn, the VV values decreased from −8 to −12 dB, and VH values also decreased from −17 to −19 dB.

Entering the late June phase, soybean plants undergo distinct stages of stem elongation and blossom development, while corn concurrently enters the tasseling phase. This period is marked by a significant augmentation in the biomass of both crops, thereby culminating in an observable escalation in backscattering values. Specifically, VV values for soybeans exhibit an incremental shift from −12 to −7 dB, whereas VH values experience a corresponding shift from −20 to −14 dB. In parallel, for corn, VV values demonstrate a transition from −12 to −7 dB, and VH values elevate from −19 to −14 dB. However, as entering early July, backscattering values begin to decrease during the late stage of stem elongation in the crops. At this point, stem density increases, and the density of leaves and branches reaches a point where the ground is almost entirely covered by the crops. This situation leads to multiple scattering of incident waves within the crop and between the crop canopy and the soil. The growing number of branches and stems results in an overall reduction in scattering, while the scattering contribution of the canopy itself remains relatively stable. Subsequently, from July to early September, as both soybean and corn attain their peak heights and biomass levels, the structural attributes of the crops demonstrate a degree of uniformity and stability.

In particular, soybean stabilizes after a slight increase, with VV values fluctuating around −8 dB and VH values around −15 dB. For corn, both VV and VH values fluctuate around −10 and −16 dB. The summer crops are typically harvested across late September and October, leading to a dominant scattering contribution from the ground. VH values decrease due to the removal of the crop canopy, while VV values increase as the recovered ground signal arises from the dryness of the vegetation in the mature period and crop residue generated after harvest.

For winter crops (winter wheat), it exhibits a distinctive planting pattern. From May to early June, as the temperature begins to rise, there is a slight increase in backscattering values (VV values increase from −13 to −12 dB, VH values increase from −19 to −17 dB). During this period, winter wheat undergoes a transition from the tillering stage to the heading stage, with the final leaf attaining full growth, leading to an augmentation in biomass. By mid-June, the leaf area of winter wheat reaches its peak, completely concealing the soil, and scattering mainly emanates from the leaf surfaces. Consequently, there is a rapid decline in backscattering coefficients during this phase. In late June, winter wheat progresses into the early milk-ripening stage with rapid spikelet growth, which leads to an upward trend in backscattering values. As July arrives, winter wheat reaches maturity and is harvested, resulting in a decrease (VV values decreased from −11 to −13 dB and VH values decreased from −15 to −20 dB). Following this, sections of the wheat fields are rendered barren by weeds, while other parts are cultivated with alfalfas. In October, in anticipation of the impending snow season in November, preparations for a new crop planting cycle commence. Plowing practices are implemented during this period, leading to the removal of weeds and alfalfas. These actions contribute to the gradual smoothening of the soil surface and a reduction in its roughness. Consequently, a decrease in backscatter values is observed in October, with VV values dropping from −9 to −11 dB, and VH values decreasing from −16 to −18 dB.

The dynamic scattering mechanisms inherent in different growth stages of the three primary agricultural crops give rise to discernible variations in the backscattering values, forming the fundamental basis for crop classification utilizing SAR data [15]. Notably, soybean and corn share similar constituents, encompassing leaves, stems, and fruits, culminating in analogous alterations in their backscattering patterns. The distribution of spikes and the structural characteristics of spikes in winter wheat resulted in some attenuation of backward scattering.

B. Coherence

Temporal evolutions of coherence are depicted in Fig. 5. Overall, the coherence under different polarization channels has a similar trend, with coherence values exceeding 0.2. The dynamics clearly show that VV polarization exhibits a heightened level of coherence in comparison to VH polarization, with VV values spanning from 0.25 to 0.55, while VH values range between 0.25 and 0.35. The popular explanation for this is divided into two main aspects. First, copolarization intensifies the sensitivity of vegetation scattering and canopy penetration, resulting in amplified backscatter and an improved signal-to-noise ratio (SNR). Second, the influence of cross polarization in the C-band relies predominantly on the vegetation layer rather than the ground layer for the echo signals originating from the study site, rendering VH polarization more vulnerable to temporal interference [57]. In April, within the study region characterized by a snow-covered landscape, all crops exhibited elevated levels of coherence. As crops from different growing seasons gradually begin to seed and flourish after the ice melts, differences between summer crops (soybean and corn) and winter crop (winter wheat) become apparent.

In the context of summer crops such as soybean and corn, the May period signifies the initial growth stages of planting these crops as the land gradually becomes covered with new shoots. The continuous and dynamic changes in the agricultural fields during our observations resulted in a modest decrease in coherence. For soybean, the VV values dropped from 0.46 to 0.37, and VH values declined from 0.30 to 0.26. Similarly, for corn, the VV values decreased from 0.49 to 0.38, and VH values fell from 0.29 to 0.26. This decrease in coherence continued until early June, whereas backscattering values increased due to a higher SNR. However, from late June to July, corresponding to the soybean stem elongation stage and corn nodulation stage, both crops exhibited their lowest average coherence levels. This decrease can be attributed to the ongoing changes in crop growth dynamics [36]. Until early September, just before the crops were about to be harvested, the coherence values fluctuated within a narrow range, with VV and VH values oscillating between 0.2 and 0.3. During September and October, within the harvesting season, the coherence values experienced a significant increase, triggered by the harvesting of crops and the subsequent revival of soil effects. The level of improvement exceeded 0.1, with corn displaying the highest coherence value ($\rho_{VV} = 0.56$, $\rho_{VH} = 0.34$), followed by soybean ($\rho_{VV} = 0.45$, $\rho_{VH} = 0.35$).

For winter crop (winter wheat), the period from May to June is significant. During this time, as the snow and ice completely melt and winter wheat rapidly grows to the tillering stage, the vegetation landscape undergoes dynamic changes, resulting in a significant decrease in coherence values (from 0.37 to 0.27 for VV and from 0.27 to 0.24 for VH). Late June marks the milk-ripening stage for winter wheat, during which the average coherence values for all crops reach their lowest points. This decrease in coherence is a result of the ongoing changes in crop growth, causing coherence values to fluctuate within a lower range, with both VV and VH values oscillating between 0.2 and 0.3. In July, winter wheat reaches maturity and is harvested, showing a slight increase in coherence. Minor coherence fluctuations occur due to the farming activities in September and early October. It can be observed that coherence significantly increases in late October (from 0.26 to 0.42 in VV and from 0.24 to 0.34 in VH). The subsequent increase is attributed to the absence of agricultural activities on the land at this stage in preparation for the winter season.

Throughout the entire phenological stage, the coherence time series of various crops under VH polarization exhibit a similarity, which reduced the separability of the crops. This suggests that the VH coherence feature is of limited use for crop classification

TABLE IV
CLASSIFICATION ACCURACY USING BACKSCATTERING BASED ON DIFFERENT POLARIZATIONS

	VV		VH		VV+VH	
Class	**PA (%)**	**UA (%)**	**PA (%)**	**UA (%)**	**PA (%)**	**UA (%)**
Soybean	95.22 ± 2.11	95.37 ± 2.07	95.85 ± 3.31	95.18 ± 1.77	97.64 ± 1.71	96.11 ± 1.66
Corn	96.61 ± 2.42	95.15 ± 3.90	96.10 ± 2.54	94.82 ± 2.93	97.05 ± 2.28	96.34 ± 3.02
Wheat	74.94 ± 13.95	81.67 ± 2.46	89.99 ± 5.61	88.70 ± 5.82	88.68 ± 8.44	91.61 ± 3.80
Forage	65.72 ± 9.73	73.14 ± 9.57	61.71 ± 6.04	75.33 ± 11.04	72.82 ± 7.34	82.76 ± 8.09
Forest	94.08 ± 3.27	91.17 ± 5.36	98.89 ± 0.47	96.50 ± 0.99	98.29 ± 1.84	97.03 ± 0.97
	OA (%)	92.33 ± 1.63	OA (%)	93.48 ± 1.53%	OA (%)	95.12 ± 1.30
	Kappa	0.88 ± 0.03	Kappa	0.90 ± 0.03	Kappa	0.93 ± 0.02

in our region. In contrast, although the VV curves of each crop display some overlap in the mid-growth stage, there were differences between crops during the plowing phase (April) and the peak of the harvest season (October), which is consistent with [34] and [35]. Therefore, it is crucial to selectively employ these coherence features to enhance the accuracy of crop classification as supplemental factors.

It is worth noting that the changes in coherence and backscattering values in the time series are strongly correlated with each other. The main reason for this phenomenon is that when vegetation is present, the backscattering signal is strengthened, indicating a decrease in coherence due to temporal decorrelation. When there is no vegetation, surface scattering from bare soil due to surface roughness and moisture results in higher intensity values but also higher coherence due to temporal stability. Based on the time series curves of backscattering and coherence, it is evident that there is a clear correlation between field observation data and estimated coherence and backscattering values in determining different phenological stages of selected crop types in the study area.

IV. RESULTS

For evaluating classification performance with diverse feature sources, we conducted three categories of classification experiments, including only backscattering, interferometric coherence alone, and a combination of both. In each category, various classification schemes have been constructed, depending on the input features, which vary in polarization and the number of images. Therefore, in order to ensure the completeness of the classification in the study site, we considered seven classes of land covers in the classification process and thematic mapping. However, due to the small sample numbers of build-up and others, these two classes were excluded from the analysis of the results.

A. Classification Using Backscattering

The initial phase of the classification evaluation exclusively employs backscattering intensity as input parameters for the RF classifier. A set of classification schemes was designed depending on backscattering from different polarization channels and SAR image numbers.

1) Influence of Polarization: To examine the influence of different polarizations on the accuracy of crop-type classification based on the backscattering intensity, three classification schemes were constructed: VV backscattering intensity, VH backscattering intensity, and a combination of both polarizations (VV + VH). To emphasize the quantitative analysis of vegetation targets, Table IV, obtained from the confusion matrix in Fig. 6, selectively presents the accuracy for five categories of vegetation across diverse polarization, where "±" is the STD computed as the average of the accuracies resulting from five times of classification experiments depending on different training and testing set.

It is clear to see that with backscattering intensity from a single polarization channel, the OA values for classification using only VV or VH are greater than 90%. Nevertheless, VH provided refined classification results than VV, achieving an OA value of 93.48% and a Kappa coefficient of 0.90, with an OA of 1.15% higher than VV. As using backscattering intensity form both polarization channels (VV + VH), the best classification performance is achieved, with an OA value of 95.12% and a Kappa coefficient of 0.93, which further improves 1.64% of OA than VH. The results highlight the remarkable capability of Sentinel-1 backscattering to capture the intricate biophysical features of crops at different growth stages, leading to accurate classification. In addition, incorporating intensities from both polarization channels as input characteristics can further improve the precision of classification. The classification maps corresponding to the different polarization channels exhibiting the best accuracy among the five predictions are shown in Fig. 6. From the visualization, it is evident that the clustering pattern resulting from polarization combinations is superior to the results obtained from single polarizations, exhibiting fewer scattered errors and clear field boundaries.

When examining the PA and UA for individual crops, it is evident that corn and soybean achieved over 95% accuracy in single polarization. However, winter wheat had limited classification performance and showed differences between various polarizations. In VV, a PA value of 74.94% and a UA value of 81.67% are observed, whereas an improved PA value of 89.99% and a UA value of 88.70% are achieved in VH, marking a notable increase of 15.05% and 7.03%. This arises from the fact that VV excels in capturing vertical vegetation structure information, while using cross polarization (HV and VH) enables the better capture of data

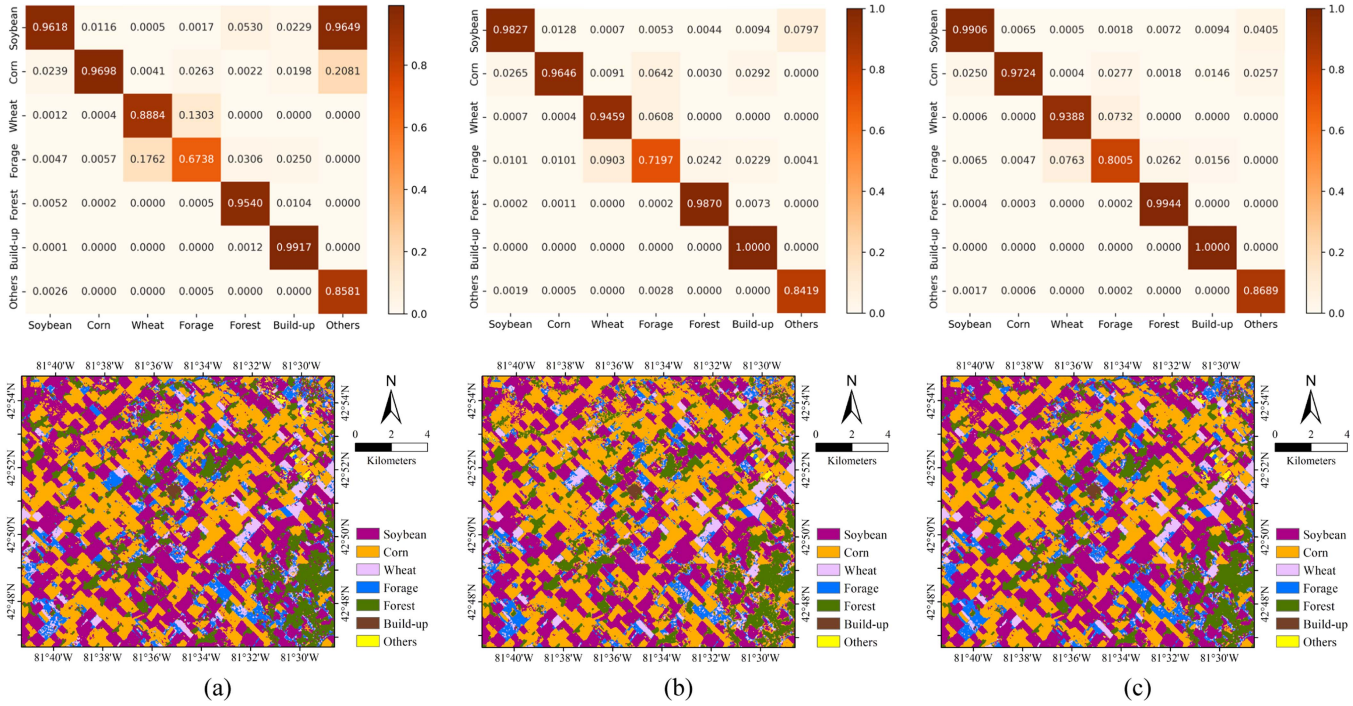

Fig. 6. Confusion matrix and classification maps with backscattering intensity images and RF algorithm using different polarization. (a) VV. (b) VH. (c) VV + VH.

pertaining to crown volume and plant biomass [58]. During the growth trajectory of winter wheat, it shows dense aggregation, rendering SAR imagery predominantly capable of capturing intricate details pertaining to the canopy. Consequently, VH unveils heightened sensitivity, thereby rendering it remarkably effective in the accurate classification of winter wheat crops. Likewise, it is worth noting that VH consistently yields superior classification accuracy within forested regions, showcasing an impeccable PA value of 98.89%.

The benefits of using a combination of VV and VH polarizations are apparent in the enhanced classification accuracies for nearly all crop species. Notably, PA and UA values for soybean and corn have both increased to exceed 97% and 96%, respectively. The UA value for winter wheat has risen to 91.61%, with only 1.31% decrease compared to VH polarization. Among the three schemes, the forage class, characterized by its perennial and varied vegetation, exhibits a more intricate structure, resulting in lower classification accuracy. Under VV + VH, the UA value barely exceeds 80%. In contrast, the classification results for forested regions are highly favorable, with both PA and UA values exceeding 90%.

2) Influence of Image Number: The number of images used to create SAR time-series data plays a crucial role in determining classification accuracy [15], [52]. Hence, we performed a sequential addition of multitemporal images from April to October 2018, and subsequently tested the classification performance with various polarization channels. Table V provides the details and classification accuracies for different combinations of time-series data. The OA values with two scenes are 43.95% and 45.43% for VV and VH polarizations. As the number of images increases, more significant improvements in classification accuracy become evident. Nevertheless, when the number of scenes exceeds 11, the incremental improvements in OA gradually diminish.

To facilitate visual comparison between VV and VH, Fig. 7 illustrates the relationship between the number of images and OA for both polarizations, where the shaded area is STD of the five classification tests for each group of increasing images as classification features. Until July 9, the accuracy in VH consistently outperforms those in VV, with a 6% difference in OA. This observation aligns with the earlier analysis of individual crop accuracy, where the sensitivity of VV to vertical structure posed challenges in discriminating winter wheat. It is worth mentioning that there is an interesting shift that occurs after adding an image on July 21 (from scenario 9 to scenario 10), leading to a significant 16% increase in accuracy in VV. This boost can be primarily attributed to the winter wheat harvest during this period, which reduces ambiguities between winter wheat and other classes. As the number of images continues to increase, the gap in accuracy between VH and VV gradually diminishes, converging to around 1% by the end. These results confirm the effectiveness of time series backscattering coefficients for crop classification [52], with temporal features outweighing backscattering features for classification accuracy.

B. Classification Using Coherence

Before evaluating the additional benefits of coherence features in crop classification, it is essential to first assess the performance when utilizing coherence features as input parameters independently [44]. A variety of classification schemes were developed based on coherences derived from different

TABLE V
RELATIONSHIP BETWEEN THE NUMBER OF IMAGES AND THE CLASSIFICATION ACCURACY

Combination	Scenarios	VV		VH	
		OA (%)	Kappa	OA (%)	Kappa
0404–0416	2	43.95 ± 1.97	0.12 ± 0.03	45.43 ± 0.35	0.15 ± 0.01
0404–0428	3	49.17 ± 3.38	0.21 ± 0.05	53.59 ± 2.39	0.28 ± 0.04
0404–0510	4	54.95 ± 1.57	0.31 ± 0.02	58.35 ± 3.17	0.36 ± 0.05
0404–0522	5	61.32 ± 1.77	0.41 ± 0.03	66.48 ± 4.91	0.49 ± 0.07
0404–0603	6	64.21 ± 1.55	0.46 ± 0.03	70.37 ± 3.62	0.55 ± 0.05
0404–0615	7	67.86 ± 2.87	0.51 ± 0.05	72.77 ± 4.49	0.58 ± 0.07
0404–0627	8	69.00 ± 2.57	0.53 ± 0.04	74.00 ± 4.25	0.6 ± 0.06
0404–0709	9	71.12 ± 3.83	0.56 ± 0.06	77.42 ± 4.35	0.66 ± 0.07
0404–0721	10	87.31 ± 2.79	0.81 ± 0.04	81.34 ± 3.95	0.72 ± 0.06
0404–0802	11	88.59 ± 2.48	0.83 ± 0.04	85.02 ± 2.31	0.77 ± 0.03
0404–0814	12	89.11 ± 2.15	0.84 ± 0.03	86.31 ± 1.66	0.79 ± 0.03
0404–0826	13	89.91 ± 1.92	0.85 ± 0.03	87.22 ± 1.31	0.81 ± 0.02
0404–0907	14	90.64 ± 1.65	0.86 ± 0.03	89.64 ± 1.28	0.84 ± 0.02
0404–0919	15	90.70 ± 1.90	0.86 ± 0.03	91.10 ± 1.25	0.86 ± 0.02
0404–1001	16	91.18 ± 2.10	0.87 ± 0.03	91.39 ± 0.51	0.87 ± 0.01
0404–1013	17	92.00 ± 1.76	0.88 ± 0.03	92.87 ± 1.53	0.89 ± 0.02
0404–1025	18	92.33 ± 1.63	0.88 ± 0.03	93.48 ± 1.67	0.90 ± 0.03

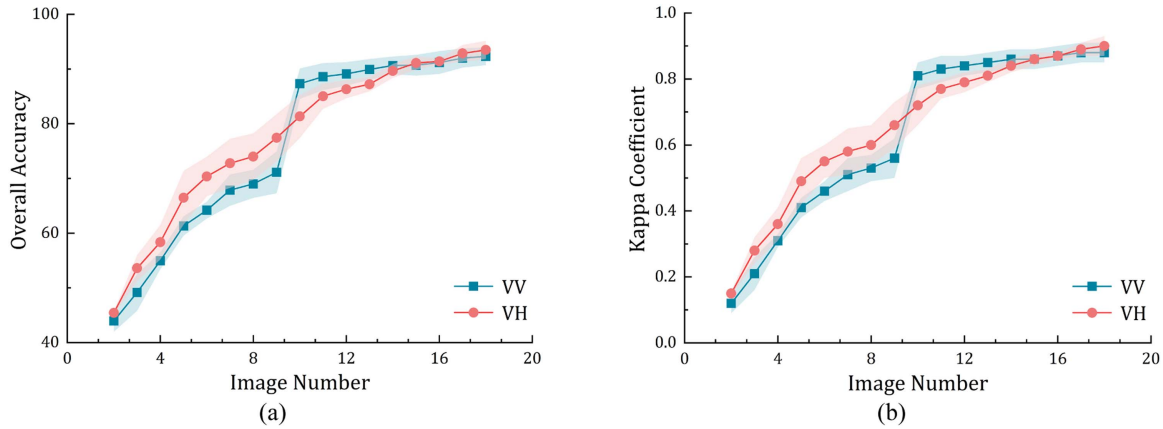

Fig. 7. Relationship between number of intensity images and classification accuracy. (a) OA. (b) Kappa.

polarization channels and phenological stages. The coherence features employed in this study were derived from Sentinel-1 interferometric pairs with 12-day intervals.

1) Influence of Polarization: To assess the impact of different polarization choices on the precision of crop-type classification through interferometric coherence, three classification schemes were created: one based on VV coherence, another on VH coherence, and a third combining both polarizations (VV + VH) coherence. The performance of these schemes was assessed by analyzing confusion matrices (see Fig. 8), and the PA and UA values for vegetation targets under various polarization combinations are presented in Table VI.

As anticipated, relying solely on coherence features for overall performance proves insufficient reflected in unsatisfactory OA values across all three schemes. The accuracy is lower than the previous study in [44], which may be attributed to a longer temporal baseline (12 days instead of 6 days). Notably, VV yields more accurate results, with an OA of 69.46% and a Kappa coefficient of 0.52. Conversely, due to the presence of lower SNR for VH coherence [47], it produces worse outcomes, exhibiting a lower OA value of 50.64% and a reduced Kappa coefficient of 0.18. This indicates the inadequacy of VH coherence for crop classification in the study area. Furthermore, combining the features in both polarizations (VV + VH) results in an OA

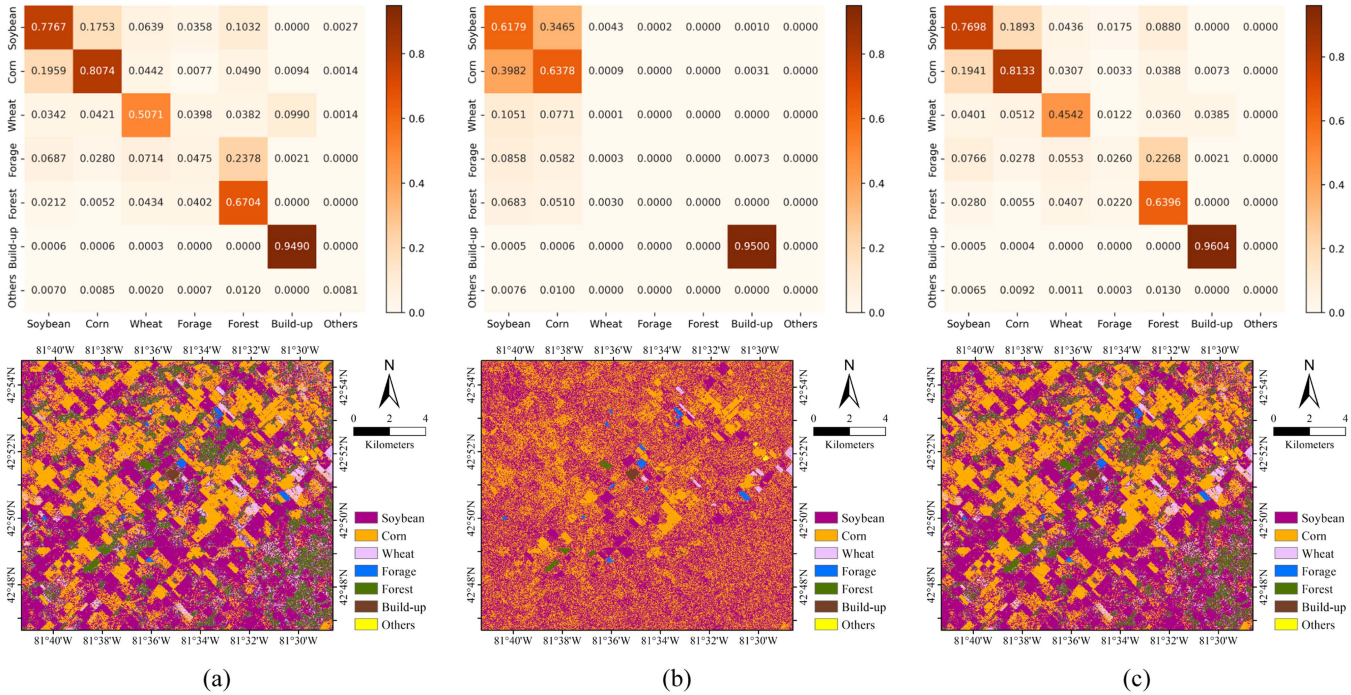

Fig. 8. Confusion matrix and classification maps with coherence images and RF algorithm using different polarizations. (a) VV. (b) VH. (c) VV + VH.

TABLE VI
CLASSIFICATION ACCURACY USING COHERENCE BASED ON DIFFERENT POLARIZATIONS

	VV		VH		VV+VH	
Class	**PA (%)**	**UA (%)**	**PA (%)**	**UA (%)**	**PA (%)**	**UA (%)**
Soybean	74.94 ± 3.58	67.27 ± 2.22	61.84 ± 4.68	46.7 0± 1.37	75.23 ± 3.87	66.15 ± 2.17
Corn	79.15 ± 4.33	74.97 ± 2.15	61.76 ± 5.90	54.3 3± 0.74	79.87 ± 4.44	74.28 ± 2.50
Wheat	41.00 ± 11.02	66.82 ± 7.14	0.02 ± 0.03	5.07 ± 10.50	37.60 ± 9.83	70.90 ± 7.01
Forage	6.71 ± 3.28	24.23 ± 4.47	0.00 ± 0.00	0.00 ± 0.00	4.17 ± 2.66	27.82 ± 9.03
Forest	63.70 ± 2.79	56.57 ± 5.91	0.00 ± 0.00	0.35 ± 0.71	61.14 ± 1.92	57.38 ± 5.66
	OA (%)	69.46 ± 1.68	OA (%)	50.64 ± 0.84	OA (%)	69.34 ± 1.59
	Kappa	0.52 ± 0.03	Kappa	0.18 ± 0.01	Kappa	0.52 ± 0.03

comparable to that of VV coherence, albeit with a marginal decrease of only 0.12%.

In Fig. 8, thematic maps are presented, showcasing the classification results across various polarization channels. The classification maps for all three schemes encountered challenges in accurately delineating crop fields, with evident scattered errors in most areas. Particularly, VH demonstrated the least effective classification performance, displaying distinct granular patterns that only partially identified major cash crops such as soybean and corn. Contrastingly, the results from the remaining two classification approaches (VV and VV + VH) exhibit relative similarity. Despite not achieving ideal performance, they offer a more comprehensive extraction of boundaries for certain farmlands.

Among the two distinct polarizations individually, soybean and corn stand out as leaders in classification accuracy, demonstrating a moderate level of precision where PA values exceed UA values. Specifically, when examining the coherence from the VH channel, the PA and UA values for soybean and corn are approximately 15% lower than those of the VV polarization. This discrepancy could be attributed to the inherent similarity within the coherence time-series data related to various crops, resulting in a scenario where the error of commission surpasses the error of omission.

For winter wheat, VV polarization showcased elevated accuracy levels, yielding PA and UA values of 41.00% and 66.82%, respectively. In contrast, VH polarization witnessed a significant decrease in classification accuracy, dropping by over 40% for both PA and UA values. This indicates that the coherence is prone to causing omission and commission errors in the classification of winter wheat. Table VI clearly indicates that the performance of the remaining land-cover categories was unsatisfactory. The forage is identified as the crop with the least effective classification, none polarization succeeded

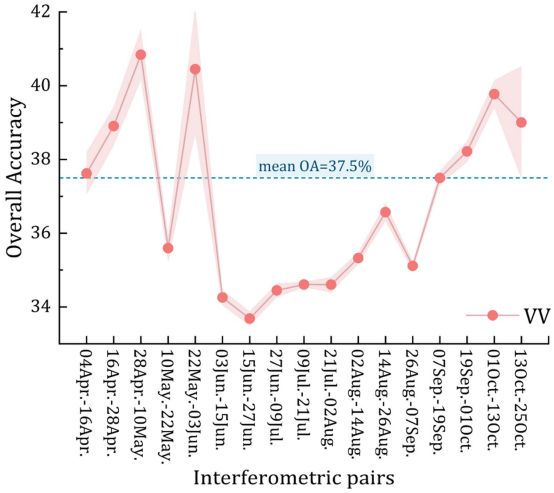

Fig. 9. Variation curve of OA using VV coherence time-series for 17 interferometric pairs individually.

in effectively distinguishing herbaceous plants. This challenge can be attributed to two factors: the relatively small number of samples for forage and the intricate complexity of forage vegetation. Regarding the identification of forested areas, VV polarization emerged as relatively reliable, boasting a PA value of 63.70%, whereas the PA value for VH polarization is only 0.00%. The lackluster performance of forests in VH polarization is partly due to the limited number of samples. In addition, low coherences in forests, especially in VH polarization, hinder their ability to provide the necessary distinctiveness for differentiation from other crops.

2) Influence of Phenology: In both the considerable number of existing studies and our work, one of the added values provided by coherence is the increased sensitivity to the early growth and harvesting stages of the crop [35], [36]. Crop phenology influences temporal coherence, consequently impacting the classification results using coherence [34]. To assess the influence of phenology on classification, we obtained the OA of classification for each interferometric pair in VV. Fig. 9 shows the relationship between the acquisition dates of image pairs and OA. It is clear that coherence with higher OA value is distributed in the early crop growth and harvest periods, which is consistent with [42]. An interesting point is that interferometric pairs with high OA values consistently exhibit high coherence values in the coherence time series curves. Using the mean OA value (37.5% in our case) as a threshold, 8 of the 17 interferometric pairs were above the threshold.

To further evaluate the performance by combining fewer coherences at key phenology, a subset of coherences in VV was constructed using the eight interferometric pairs as new input for classification. Table VII demonstrates the accuracy before and after selection. It is evident that the difference in accuracy between them is negligible, with a 2.31% decrease in OA using the subset. This suggests that coherence from a few interferometric pairs on specific dates can produce comparable classification results while reducing the cost burden and improving computational efficiency.

TABLE VII
CLASSIFICATION ACCURACY OF TIME-SERIES SETS BEFORE AND AFTER SELECTION BASED ON VV COHERENCE

	VV		VV-selected	
Class	**PA (%)**	**UA (%)**	**PA (%)**	**UA (%)**
Soybean	74.94 ± 3.58	67.27 ± 2.22	73.58 ± 3.00	64.81 ± 1.91
Corn	79.15 ± 4.33	74.97 ± 2.15	77.10 ± 5.02	74.16 ± 2.28
Wheat	41.00 ± 11.02	66.82 ± 7.14	32.37 ± 6.20	56.57 ± 9.24
Forage	6.71 ± 3.28	24.23 ± 4.47	5.98 ± 2.66	21.67 ± 5.85
Forest	63.70 ± 2.79	56.57 ± 5.91	59.95 ± 1.02	52.70 ± 6.27
	OA (%)	69.46 ± 1.68	OA (%)	67.15 ± 1.63
	Kappa	0.52 ± 0.03	Kappa	0.49 ± 0.02

C. Classification Using Backscattering and Coherence

While the classification results based on coherence alone fall significantly short compared to those obtained using backscattering in prior experiments, it is worthwhile to integrate both backscattering and coherence features to explore the additional value coherence may bring to crop classification [42]. Three schemes were implemented, combining features from both backscattering and coherence, aiming to evaluate the supplementary impact of coherence across different polarization channels. Table VIII lists the mean values of each accuracy calculated from the confusion matrix (see Fig. 10) of the five classification tests, illustrating the classification accuracy metrics for vegetation targets in various polarization combinations (VV, VH, and combinations of both). When compared with the results presented in Table IV (backscattering only) and Table VI (coherence only), it becomes evident that integrating interferometric coherence with SAR backscattering significantly improves crop classification accuracy. Particularly noteworthy is the outstanding separability of soybean, corn, and forested regions, achieving classification accuracies surpassing 95% within these three schemes.

In comparison to the coherence feature set with the same polarization, all schemes incorporating combined features exhibit significant improvements in classification accuracy [42], [44]. In contrast to individual backscattering features, VV leads to the most significant OA improvement at 1.00%, while VH and VV + VH result in minor OA enhancements of 0.31% and 0.20%, respectively. Moreover, the inclusion of the VV coherence resulted in the most substantial increase in both PA and UA values for each crop. Specifically, the PA value for winter wheat reflected a remarkable increase of 4.43% (from 74.94% to 79.37%). Similarly, the PA value for forage increased from 65.72% to 69.90%, indicating an improvement of 4.18%. This observation is consistent with the earlier analysis in Section IV-B, emphasizing the classification benefits of VV coherence over VH coherence. Finally, the most effective classification result is obtained with the strategy that integrates both backscattering and coherence attributes from both polarizations, achieving an OA of 95.32% and a kappa coefficient of 0.93. The classification maps for the three schemes are illustrated in Fig. 10. This scheme accurately delineates the boundaries of each parcel with minimal errors.

TABLE VIII
CLASSIFICATION ACCURACY USING BOTH BACKSCATTERING AND COHERENCE FEATURES BASED ON DIFFERENT POLARIZATIONS

	VV		VH		VV+VH	
Class	**PA (%)**	**UA (%)**	**PA (%)**	**UA (%)**	**PA (%)**	**UA (%)**
Soybean	96.06 ± 1.42	95.43 ± 1.96	96.15 ± 2.92	95.27 ± 1.79	97.72 ± 1.74	96.10 ± 1.70
Corn	96.82 ± 2.33	96.50 ± 3.55	96.34 ± 2.45	94.80 ± 2.87	97.11 ± 2.26	96.49 ± 2.88
Wheat	79.37 ± 10.12	85.47 ± 2.16	90.03 ± 5.75	89.75 ± 5.16	89.15 ± 8.10	92.20 ± 3.17
Forage	69.90 ± 12.02	75.93 ± 8.23	62.59 ± 6.60	77.14 ± 9.98	73.43 ± 8.29	82.93 ± 9.44
Forest	96.68 ± 1.25	96.43 ± 1.83	99.31 ± 0.29	96.83 ± 0.55	99.34 ± 0.69	97.45 ± 0.83
	OA (%)	93.33 ± 1.29	OA (%)	93.79 ± 1.59	OA (%)	95.32 ± 1.28
	Kappa	0.90 ± 0.02	Kappa	0.91 ± 0.02	Kappa	0.93 ± 0.02

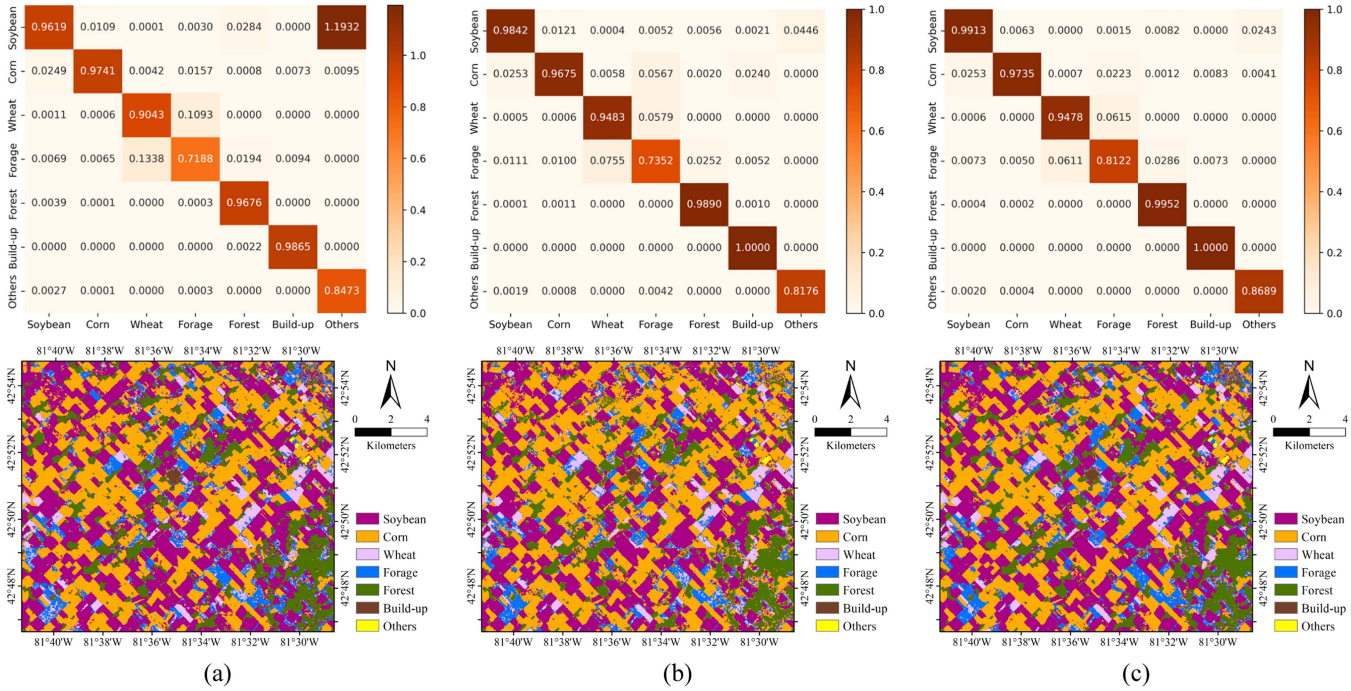

Fig. 10. Confusion matrix and classification maps using both backscattering and coherence features. (a) VV. (b) VH. (c) VV + VH.

In addition, the preceding experimental findings, as presented in Table IV for backscattering exclusively and Table VI for coherence alone, suggest that the backscattering coefficient of VV + VH and the coherence of VV yield better classification performance within a single source of features, respectively. Consequently, it is worthwhile to assess the classification scheme by integrating VV coherence with all backscattering features and to compare it with the scheme utilizing all backscattering and coherence features. As depicted in Table IX, the overall accuracies of the two classification schemes exhibit remarkably similar results, with OA values of 95.33% and 95.32%. Fig. 11 displays the confusion matrix with thematic maps for the best classification scheme of this study. There is basically no difference between the thematic maps and confusion matrices of these two schemes. The slight difference can be mainly attributed to the RF classifier and remains within a negligible range. The attainment of the desired crop classification outcome is possible by utilizing VV coherence and two backscattering coefficients with multitemporal Sentinel-1 dual-polarization data, thereby reducing feature redundancy and accelerating computation time.

V. DISCUSSION

A. Temporal Dynamics

Aligning with previous studies [14], [15], [21], our study confirmed that the temporal dynamics of backscattering coefficients can reflect changes in crop growth. The dynamic curves of different crops tend to stabilize after a period of fluctuation, before oscillating again with harvest. The fluctuation is composed of various factors, such as vegetation density, soil moisture, and roughness [58], [59]. Due to depolarization effects in VH, a significant gap was found in backscattering between VV and VH for all crops. Moreover, VV coherence fluctuates over a wide range of 0.2–0.5 in our case, while VH ranges from 0.2 to 0.3. It indicates that VH is more sensitive to crop growth than VV, consistent with the findings in the previous works [34], [37].

TABLE IX
CLASSIFICATION ACCURACY OF TIME-SERIES SETS BASED ON DIFFERENT COHERENCE ATTRIBUTES AND ALL BACKSCATTERING COEFFICIENTS

	Coherence (VV)-Backscattering (VV+VH)		Coherence (VV+VH)-Backscattering (VV+VH)	
Class	**PA (%)**	**UA (%)**	**PA (%)**	**UA (%)**
Soybean	97.43 ± 1.88	96.59 ± 1.53	97.72 ± 1.74	96.10 ± 1.70
Corn	97.83 ± 1.72	95.91 ± 2.93	97.11 ± 2.26	96.49 ± 2.88
Wheat	88.22 ± 7.04	92.90 ± 0.90	89.15 ± 8.10	92.20 ± 3.17
Forage	71.66 ± 8.73	81.67 ± 8.99	73.43 ± 8.29	82.93 ± 9.44
Forest	99.06 ± 1.23	97.30 ± 0.82	99.34 ± 0.69	97.45 ± 0.83
	OA (%)	95.33 ± 1.21	OA (%)	95.32 ± 1.28
	Kappa	0.93 ± 0.02	Kappa	0.93 ± 0.02

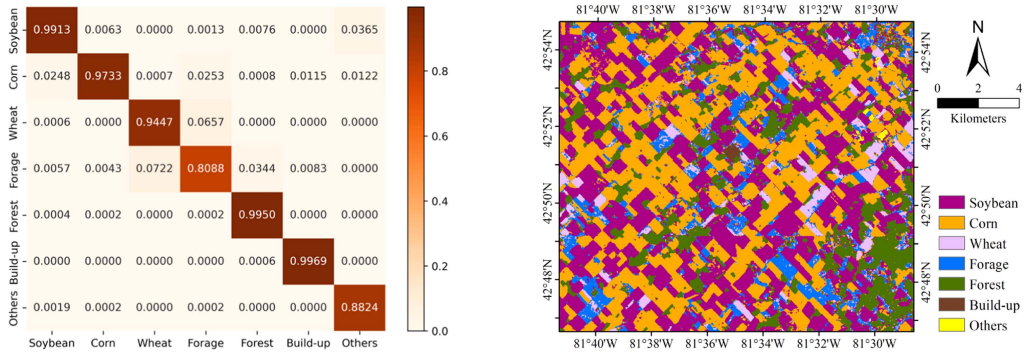

(a) (b)

Fig. 11. Confusion matrix and classification maps of the combination with backscattering coefficients of VV + VH and the coherence of VV. (a) Confusion matrix. (b) Thematic map.

The results of these studies also consolidated that coherence is a useful vegetation index for monitoring crop growth with VV coherence demonstrating higher sensitivity [35], [36]. The difference in coherence values between VV and VH was also observed, mainly due to the phase difference between the two polarizations [34], [60]. The maximum differences for the three crops in both polarizations are 0.23, 0.33, and 0.25, respectively, which are roughly consistent with the results using Sentinel-1 data acquired from track 65 in [34]. The maximum interferometric coherence value for all crops is around 0.5, mainly in April and October, similar to studies based on the same revisit cycle (12 days) [37], [40], [61]. However, Sentinel-1 images with a 6-day revisit cycle exhibit a higher coherence value (about 0.7) for the same crops [35], [44], [45], which indicates that a short temporal baseline can maintain high coherence to resist potential backscattering changes induced by factors such as regional climate variations, cultivation practices, and crop growth. In our study, we also found that the dynamic behaviors of coherence are highly correlated with the variation in backscattering with the growth of crops. In most cases, significant fluctuations in backscattering will result in a decrease in coherence, attributed to the strong temporal decorrelation. However, there are a few exceptions in our study (e.g., the InSAR pair of May 22 and June 3), which could be attributed to lower SNR decorrelation.

B. Crop Classification

The classification results using only the coherence feature are worse than using backscattering alone, with an OA of approximately 70% for the VV polarization, similar to that in [42] for a time baseline of 12 days. Although the accuracy is lower than the results obtained with a 6-day temporal baseline [44], [45], however, coherence with a 12-day revisit cycle still validates its added value to improve crop classification performance using backscattering, especially for VV. The combination of backscattering with coherence in both polarizations (VV and VH) significantly improved the accuracy of winter wheat and forage while slightly enhancing the accuracy of soybean and corn. In contrast to previous works [30], [43], [44], we found that the best crop classification scheme in our study combines the backscattering coefficients of dual polarization (VV + VH) with the VV coherence feature instead of using all four features. Moreover, an interesting point of our work is providing more detailed insights from the perspective of the number of images and the phenological period by linking temporal behavior and classification. Specifically, we found that the impact of temporal characteristics on classification accuracy narrows the gap between the two polarimetric backscattering features, and the harvest of winter wheat led to a notable enhancement in crop classification accuracy based on backscattering. Also, the interferometric pairs during phenological periods with high coherence values yield high OA. Selecting these pairs can obtain comparable results to using all pairs.

C. Limitations and Future Work

The study shows that VV coherence plays a complementary role to the backscattering coefficient, particularly in identifying

winter wheat crops with spike structures. However, our study has certain limitations as it only involves three types of crops and has a dataset with a revisit cycle of 12 days from a single orbit (Orbit 77). In future work, exploring the additional role of coherence in crop growth monitoring and mapping can be extended to more diverse crop types, even incorporating different radar frequencies (e.g., X, L, and P-band), polarization modes, and temporal baselines.

The coherence, as a crucial feature in this study, is estimated using a maximum likelihood estimator. However, it tends to be biased toward lower coherence values, employing higher values than the actual coherence [62]. This bias leads to overestimation and subsequent contrast loss. The unbiased coherence is essential for better reflecting scene changes induced by crop growth. Some solutions have been proposed to get unbiased coherence asymptotically [30], [36], [42]. In future research, we aim to explore more accurate methods for obtaining unbiased coherence and investigate its contributions to crop classification and monitoring.

It is certainly true that the current development of classifiers is very rapid, particularly, the popular deep learning provides an excellent channel for classification [54]. Deep learning can take into account both temporal and spatial features. We will consider deep learning techniques when we need to input a large number of features when we carry out multiyear, multi-data-source crop classification studies in the future. In addition, further investigations could be directed toward dynamic crop change detection based on both coherence and backscattering. This might include tasks such as identifying crop rotation, detecting changes in the same field over time, and similar analyses. These will help to grasp clearer spatial and temporal changes in crop cropping structure, which provides a basis for scientific planning and rational layout to guide agricultural production.

VI. Conclusion

In this article, we explored the application of interferometric coherence and polarimetric backscattering derived from the time series C-band Sentinel-1 SAR dataset for crop growth monitoring and classification in the agricultural region of Southwestern Ontario, Canada. As demonstrated in this study, we concentrated on understanding the temporal dynamics of three primary crops, providing insights into the behavior influencing the crop classification results. The main conclusions are drawn as follows.

1) The VH backscattering and the VV coherence show a higher sensitivity to the variations in crop growth. Moreover, the dynamics of coherence are strongly correlated with the variation of backscattering with the growth of crops.
2) The backscattering feature displays better ability in crop classification compared to coherence features. The integration of coherence with backscattering resulted in an improvement in classification accuracy. Among all classification schemes, the most effective result is achieved by combining both the backscattering of dual polarization (VV + VH) and the VV coherence, with an OA of 95.33% and a kappa coefficient of 0.93.
3) The impact of temporal characteristics on classification accuracy will reduce the difference between two backscattering features. In addition, the interferometric pairs in the phenological periods exhibiting high coherence values produce high OA values. Besides, coherence features from a few selected interferometric pairs on specific dates can produce comparable classification results.

Acknowledgment

All Sentinel-1 data used in this study were graciously provided free of charge by ESA. The reference dataset was generously supplied by the Geographic Information Technology and Applications Laboratory at the University of Western Ontario.

References

[1] L. Zhao et al., "In-season crop type identification using optimal feature knowledge graph," *ISPRS J. Photogrammetry Remote Sens.*, vol. 194, pp. 250–266, Dec. 2022, doi: 10.1016/j.isprsjprs.2022.10.017.
[2] D. M. Johnson and R. Mueller, "Pre-and within-season crop type classification trained with archival land cover information," *Remote Sens. Environ.*, vol. 264, Oct. 2021, Art. no. 112576, doi: 10.1016/j.rse.2021.112576.
[3] A. Orynbaikyzy, U. Gessner, and C. Conrad, "Crop type classification using a combination of optical and radar remote sensing data: A review," *Int. J. Remote Sens.*, vol. 40, no. 17, pp. 6553–6595, Feb. 2019, doi: 10.1080/01431161.2019.1569791.
[4] I. Becker-Reshef et al., "Strengthening agricultural decisions in countries at risk of food insecurity: The GEOGLAM crop monitor for early warning," *Remote Sens. Environ.*, vol. 237, Feb. 2020, Art. no. 111553, doi: 10.1016/j.rse.2019.111553.
[5] B. Franch et al., "Remote sensing based yield monitoring: Application to winter wheat in United States and Ukraine," *Int. J. Appl. Earth Observ. Geoinf.*, vol. 76, pp. 112–127, Apr. 2019, doi: 10.1016/j.jag.2018.11.012.
[6] O. Kavats, D. Khramov, K. Sergieieva, and V. Vasyliev, "Monitoring of sugarcane harvest in Brazil based on optical and SAR data," *Remote Sens.*, vol. 12, no. 24, Dec. 2020, Art. no. 4080, doi: 10.3390/rs12244080.
[7] M. Maimaitijiang, V. Sagan, P. Sidike, A. M. Daloye, H. Erkbol, and F. B. Fritschi, "Crop monitoring using satellite/UAV data fusion and machine learning," *Remote Sens.*, vol. 12, no. 9, Apr. 2020, Art. no. 1357, doi: 10.3390/rs12091357.
[8] M. Mahlayeye, R. Darvishzadeh, and A. Nelson, "Cropping patterns of annual crops: A remote sensing review," *Remote Sens.*, vol. 14, no. 10, May 2022, Art. no. 2404, doi: 10.3390/rs14102404.
[9] H. Yu, B. Kong, Y. Hou, X. Xu, T. Chen, and X. Liu, "A critical review on applications of hyperspectral remote sensing in crop monitoring," *Exp. Agric.*, vol. 58, Jul. 2022, Art. no. e26, doi: 10.1017/S0014479722000278.
[10] C. Liu, Z. Chen, S. Yun, J. Chen, T. Hasi, and H. Pan, "Research advances of SAR remote sensing for agriculture applications: A review," *J. Integrative Agriculture*, vol. 18, no. 3, pp. 506–525, Mar. 2019, doi: 10.1016/S2095-3119(18)62016-7.
[11] M. Busquier, J. M. Lopez-Sanchez, F. Ticconi, and N. Floury, "Combination of time series of L-, C-, and X-band SAR images for land cover and crop classification," *IEEE J. Sel. Topics Appl. Earth Observ. Remote Sens.*, vol. 15, pp. 8266–8286, 2022, doi: 10.1109/JSTARS.2022.3207574.
[12] D. Mandal, A. Bhattacharya, and Y. S. Rao, *Radar Remote Sensing For Crop Biophysical Parameter Estimation*. Berlin, Germany: Springer, 2021.
[13] M. F. Çelik and E. Erten, "Biophysical parameter estimation of crops from polarimetric synthetic aperture radar imagery with data-driven polynomial chaos expansion and global sensitivity analysis," *Comput. Electron. Agriculture*, vol. 194, Mar. 2022, Art. no. 106781, doi: 10.1016/j.compag.2022.106781.
[14] A. Veloso et al., "Understanding the temporal behavior of crops using Sentinel-1 and Sentinel-2-like data for agricultural applications," *Remote Sens. Environ.*, vol. 199, pp. 415–426, Sep. 2017, doi: 10.1016/j.rse.2017.07.015.

[15] Q. Xie et al., "Crop monitoring and classification using polarimetric RADARSAT-2 time-series data across growing season: A case study in southwestern Ontario, Canada," *Remote Sens.*, vol. 13, no. 7, Apr. 2021, Art. no. 1394, doi: 10.3390/rs13071394.

[16] Q. Xie et al., "On the use of Neumann decomposition for crop classification using multi-temporal RADARSAT-2 polarimetric SAR data," *Remote Sens.*, vol. 11, no. 7, Mar. 2019, Art. no. 776, doi: 10.3390/rs11070776.

[17] G. Satalino, F. Mattia, T. Le Toan, and M. Rinaldi, "Wheat crop mapping by using ASAR AP data," *IEEE Trans. Geosci. Remote Sens.*, vol. 47, no. 2, pp. 527–530, Feb. 2009, doi: 10.1109/TGRS.2008.2008026.

[18] X. Zhou, J. Wang, Y. He, and B. Shan, "Crop classification and representative crop rotation identifying using statistical features of time-series sentinel-1 GRD data," *Remote Sens.*, vol. 14, no. 20, Oct. 2022, Art. no. 5116, doi: 10.3390/rs14205116.

[19] C. Silva-Perez, A. Marino, J. M. Lopez-Sanchez, and I. Cameron, "Multi-temporal polarimetric SAR change detection for crop monitoring and crop type classification," *IEEE J. Sel. Topics Appl. Earth Observ. Remote Sens.*, vol. 14, pp. 12361–12374, 2021, doi: 10.1109/JSTARS.2021.3130186.

[20] Y. Shao et al., "Rice monitoring and production estimation using multitemporal RADARSAT," *Remote Sens. Environ.*, vol. 76, no. 3, pp. 310–325, Jun. 2001, doi: 10.1016/S0034-4257(00)00212-1.

[21] M. Arias, M. Á. Campo-Bescós, and J. Álvarez-Mozos, "Crop classification based on temporal signatures of Sentinel-1 observations over Navarre province, Spain," *Remote Sens.*, vol. 12, no. 2, Jan. 2020, Art. no. 278, doi: 10.3390/rs12020278.

[22] E. Beriaux, A. Jago, C. Lucau-Danila, V. Planchon, and P. Defourny, "Sentinel-1 time series for crop identification in the framework of the future CAP monitoring," *Remote Sens.*, vol. 13, no. 14, Jul. 2021, Art. no. 2785, doi: 10.3390/rs13142785.

[23] H. McNairn, J. Ellis, J. Van Der Sanden, T. Hirose, and R. Brown, "Providing crop information using RADARSAT-1 and satellite optical imagery," *Int. J. Remote Sens.*, vol. 23, no. 5, pp. 851–870, Nov. 2002, doi: 10.1080/01431160110070753.

[24] H. Skriver et al., "Crop classification using short-revisit multitemporal SAR data," *IEEE J. Sel. Topics Appl. Earth Observ. Remote Sens.*, vol. 4, no. 2, pp. 423–431, Jun. 2011, doi: 10.1109/JSTARS.2011.2106198.

[25] A. Larrañaga and J. Álvarez-Mozos, "On the added value of quad-pol data in a multi-temporal crop classification framework based on RADARSAT-2 imagery," *Remote Sens.*, vol. 8, no. 4, Apr. 2016, Art. no. 335, doi: 10.3390/rs8040335.

[26] M. S. Moran, L. Alonso, J. F. Moreno, M. P. C. Mateo, D. F. De La Cruz, and A. Montoro, "A RADARSAT-2 quad-polarized time series for monitoring crop and soil conditions in Barrax, Spain," *IEEE Trans. Geosci. Remote Sens.*, vol. 50, no. 4, pp. 1057–1070, Apr. 2012, doi: 10.1109/TGRS.2011.2166080.

[27] R. Nasirzadehdizaji, F. Balik Sanli, S. Abdikan, Z. Cakir, A. Sekertekin, and M. Ustuner, "Sensitivity analysis of multi-temporal Sentinel-1 SAR parameters to crop height and canopy coverage," *Appl. Sci.*, vol. 9, no. 4, Feb. 2019, Art. no. 655, doi: 10.3390/app9040655.

[28] M. Ioannidou, A. Koukos, V. Sitokonstantinou, I. Papoutsis, and C. Kontoes, "Assessing the added value of Sentinel-1 PolSAR data for crop classification," *Remote Sens.*, vol. 14, no. 22, Nov. 2022, Art. no. 5739, doi: 10.3390/rs14225739.

[29] S. Ge, O. Antropov, W. Su, H. Gu, and J. Praks, "Deep recurrent neural networks for land-cover classification using Sentinel-1 InSAR time series," in *Proc. IEEE Int. Geosci. Remote Sens. Symp.*, 2019, pp. 473–476.

[30] A. W. Jacob et al., "Sentinel-1 InSAR coherence for land cover mapping: A comparison of multiple feature-based classifiers," *IEEE J. Sel. Topics Appl. Earth Observ. Remote Sens.*, vol. 13, pp. 535–552, 2020, doi: 10.1109/JSTARS.2019.2958847.

[31] M. E. Engdahl and J. M. Hyyppa, "Land-cover classification using multitemporal ERS-1/2 InSAR data," *IEEE Trans. Geosci. Remote Sens.*, vol. 41, no. 7, pp. 1620–1628, Jul. 2003, doi: 10.1109/TGRS.2003.813271.

[32] X. Blaes and P. Defourny, "Retrieving crop parameters based on tandem ERS 1/2 interferometric coherence images," *Remote Sens. Environ.*, vol. 88, no. 4, pp. 374–385, Dec. 2003, doi: 10.1016/j.rse.2003.08.008.

[33] E. Ramsey III, Z. Lu, A. Rangoonwala, and R. Rykhus, "Multiple baseline radar interferometry applied to coastal land cover classification and change analyses," *GIScience Remote Sens.*, vol. 43, no. 4, pp. 283–309, 2006, doi: 10.2747/1548-1603.43.4.283.

[34] R. Nasirzadehdizaji, Z. Cakir, F. B. Sanli, S. Abdikan, A. Pepe, and F. Calo, "Sentinel-1 interferometric coherence and backscattering analysis for crop monitoring," *Comput. Electron. Agriculture*, vol. 185, Jun. 2021, Art. no. 106118, doi: 10.1016/j.compag.2021.106118.

[35] A. Villarroya-Carpio and J. M. Lopez-Sanchez, "Multi-annual evaluation of time series of Sentinel-1 interferometric coherence as a tool for crop monitoring," *Sensors*, vol. 23, no. 4, Feb. 2023, Art. no. 1833, doi: 10.3390/s23041833.

[36] A. Villarroya-Carpio, J. M. Lopez-Sanchez, and M. E. Engdahl, "Sentinel-1 interferometric coherence as a vegetation index for agriculture," *Remote Sens. Environ.*, vol. 280, Oct. 2022, Art. no. 113208, doi: 10.1016/j.rse.2022.113208.

[37] M. Barbouchi et al., "Wheat water deficit monitoring using synthetic aperture radar backscattering coefficient and interferometric coherence," *Agriculture*, vol. 12, no. 7, Jul. 2022, Art. no. 1032, doi: 10.3390/agriculture12071032.

[38] N. Ouaadi et al., "Monitoring of wheat crops using the backscattering coefficient and the interferometric coherence derived from Sentinel-1 in semi-arid areas," *Remote Sens. Environ.*, vol. 251, Dec. 2020, Art. no. 112050, doi: 10.1016/j.rse.2020.112050.

[39] J. Liu et al., "Spatiotemporal change detection of coastal wetlands using multi-band SAR coherence and synergetic classification," *Remote Sens.*, vol. 14, no. 11, May 2022, Art. no. 2610, doi: 10.3390/rs14112610.

[40] T. Tamm, K. Zalite, K. Voormansik, and L. Talgre, "Relating Sentinel-1 interferometric coherence to mowing events on grasslands," *Remote Sens.*, vol. 8, no. 10, Sep. 2016, Art. no. 802, doi: 10.3390/rs8100802.

[41] P. Castellazzi, S. Khan, S. J. Walker, R. Bartley, S. N. Wilkinson, and J. C. Normand, "Monitoring erosion in tropical savannas from C-band radar coherence," *Remote Sens. Environ.*, vol. 290, May 2023, Art. no. 113546, doi: 10.1016/j.rse.2023.113546.

[42] T. Nikaein, L. Iannini, R. A. Molijn, and P. Lopez-Dekker, "On the value of Sentinel-1 InSAR coherence time-series for vegetation classification," *Remote Sens.*, vol. 13, no. 16, Aug. 2021, Art. no. 3300, doi: 10.3390/rs13163300.

[43] M. Busquier, J. M. Lopez-Sanchez, A. Mestre-Quereda, E. Navarro, M. P. González-Dugo, and L. Mateos, "Exploring TanDEM-X interferometric products for crop-type mapping," *Remote Sens.*, vol. 12, no. 11, Jun. 2020, Art. no. 1774, doi: 10.3390/rs12111774.

[44] A. Mestre-Quereda, J. M. Lopez-Sanchez, F. Vicente-Guijalba, A. W. Jacob, and M. E. Engdahl, "Time-series of Sentinel-1 interferometric coherence and backscatter for crop-type mapping," *IEEE J. Sel. Topics Appl. Earth Observ. Remote Sens.*, vol. 13, pp. 4070–4084, 2020, doi: 10.1109/JSTARS.2020.3008096.

[45] S. Amherdt, N. C. Di Leo, A. Pereira, C. Cornero, and M. C. Pacino, "Assessment of interferometric coherence contribution to corn and soybean mapping with Sentinel-1 data time series," *Geocarto Int.*, vol. 38, pp. 1–22, Nov. 2022, doi: 10.1080/10106049.2022.2144472.

[46] R. Bamler and P. Hartl, "Synthetic aperture radar interferometry," *Inverse Problems*, vol. 14, no. 4, 1998, Art. no. R1, doi: 10.1088/0266-5611/14/4/001.

[47] H. A. Zebker and J. Villasenor, "Decorrelation in interferometric radar echoes," *IEEE Trans. Geosci. Remote Sens.*, vol. 30, no. 5, pp. 950–959, Sep. 1992, doi: 10.1109/36.175330.

[48] ESA-SNAP Development Team, "Sentinel application platform software." Accessed: Aug. 27, 2022. [Online]. Available: http://step.esa.int/main/toolboxes/snap

[49] T. G. Dietterich, "An experimental comparison of three methods for constructing ensembles of decision trees: Bagging, boosting, and randomization," *Mach. Learn.*, vol. 40, pp. 139–157, Aug. 2000.

[50] L. Breiman, "Random forests," *Mach. Learn.*, vol. 45, pp. 5–32, Oct. 2001.

[51] F. Pedregosa et al., "Scikit-learn: Machine learning in python," *J. Mach. Learn. Res.*, vol. 12, pp. 2825–2830, Oct. 2011.

[52] C. Liao, J. Wang, X. Huang, and J. Shang, "Contribution of minimum noise fraction transformation of multi-temporal RADARSAT-2 polarimetric SAR data to cropland classification," *Can. J. Remote Sens.*, vol. 44, no. 3, pp. 215–231, Nov. 2018, doi: 10.1080/07038992.2018.1481737.

[53] S. Hariharan, D. Mandal, S. Tirodkar, V. Kumar, A. Bhattacharya, and J. M. Lopez-Sanchez, "A novel phenology based feature subset selection technique using random forest for multitemporal PolSAR crop classification," *IEEE J. Sel. Topics Appl. Earth Observ. Remote Sens.*, vol. 11, no. 11, pp. 4244–4258, Nov. 2018, doi: 10.1109/JSTARS.2018.2866407.

[54] L. Zhong, L. Hu, and H. Zhou, "Deep learning based multi-temporal crop classification," *Remote Sens. Environ.*, vol. 221, pp. 430–443, Feb. 2019, doi: 10.1016/j.rse.2018.11.032.

[55] J. Cohen, "A coefficient of agreement for nominal scales," *Educ. Psychol. Meas.*, vol. 20, no. 1, pp. 37–46, Apr. 1960, doi: 10.1177/001316446002000104.

[56] M. Story and R. G. Congalton, "Accuracy assessment: A user's perspective," *Photogrammetry Eng. Remote Sens.*, vol. 52, no. 3, pp. 397–399, Mar. 1986.

[57] R. Manavalan, "Review of synthetic aperture radar frequency, polarization, and incidence angle data for mapping the inundated regions," *J. Appl. Remote Sens.*, vol. 12, no. 2, p. 021501, May 2018, doi: 10.1117/1.jrs.12.021501.

[58] D. Mandal et al., "Dual polarimetric radar vegetation index for crop growth monitoring using Sentinel-1 SAR data," *Remote Sens. Environ.*, vol. 247, Sep. 2020, Art. no. 111954, doi: 10.1016/j.rse.2020.111954.

[59] J. R. Wang, E. T. Engman, T. Mo, T. J. Schmugge, and J. C. Shiue, "The effects of soil moisture, surface roughness, and vegetation on L-band emission and backscatter," *IEEE Trans. Geosci. Remote Sens.*, vol. GE-25, no. 6, pp. 825–833, Nov. 1987, doi: 10.1109/TGRS.1987.289754.

[60] H. McNairn, C. Duguay, B. Brisco, and T. J. Pultz, "The effect of soil and crop residue characteristics on polarimetric radar response," *Remote Sens. Environ.*, vol. 80, no. 2, pp. 308–320, May 2002, doi: 10.1016/S0034-4257(01)00312-1.

[61] A. Pandit, S. Sawant, J. Mohite, and S. Pappula, "Sentinel-1-derived coherence time-series for crop monitoring in Indian agriculture region," *Geocarto Int.*, vol. 37, no. 25, pp. 9497–9517, Jan. 2022, doi: 10.1080/10106049.2021.2022008.

[62] R. Touzi, A. Lopes, J. Bruniquel, and P. W. Vachon, "Coherence estimation for SAR imagery," *IEEE Trans. Geosci. Remote Sens.*, vol. 37, no. 1, pp. 135–149, Jan. 1999, doi: 10.1109/36.739146.